AAS 15-756

MISSION DESIGN ANALYSIS FOR THE MARTIAN MOON PHOBOS: CLOSE FLYBYS, MISSED THRUSTS, AND OTHER IN-FLIGHT ENTERTAINMENT

Jeffrey Stuart,[*] Tim McElrath,[†] and Anastassios Petropoulos[‡]

A robotic mission to the Martian moons Phobos and Deimos would offer a wealth of scientific information and serve as a useful precursor to potential human missions. In this paper, we investigate a prospective mission enabled by solar electric propulsion that would explore Phobos via a series of flybys followed by capture into orbit around the moon. Of particular interest are low-cost options for capture and walkdown to the target science orbits aided by multi-body effects due to the mutual gravitational interaction of Phobos and Mars. We also consider contingency operations in the event of missed thrust or maneuver execution errors.

INTRODUCTION

The Martian moons Phobos and Deimos are of great scientific interest in and of themselves and (in the case of Phobos) present a potential staging area for future human exploration of Mars.[1] Indeed, the origin of these irregularly shaped bodies, so similar in composition to C-type asteroids but in such close proximity to a major gravitational body, is still a controversial topic of discussion.[2] Thus, resolving whether the moons were formed around Mars via accretion or are captured bodies can provide valuable insight into the early history and evolution of Mars and the solar system as a whole. To date, however, there have been few successful missions devoted to exploring these bodies, though tantalizing observations are often made by dedicated Mars missions.[3] Accordingly, we investigate a mission concept for robotic exploration wherein a spacecraft with an ion propulsion system will explore Phobos via a series of flybys followed by eventual capture into a Phobos-centric mapping orbit. In particular, we consider avenues for capture about Phobos, a walkdown to the target science orbits, and contingency operations for events such as missed thrusts or thruster errors are analyzed. Even though the proposed concept is not itself a lander mission, this investigation also provides key insights into the mission design and navigation of future sample return or human missions.

Given the notional orbital campaign, a number of key mission design and navigation considerations are readily identified. In particular, due to the relative sparsity of observations, the shape and

[*]Navigation and Mission Design System Engineering Group, Mission Design and Navigation Section, Jet Propulsion Laboratory, California Institute of Technology, 4800 Oak Grove Dr., Pasadena, CA 91109, (818) 354-0071, jeffrey.r.stuart@jpl.nasa.gov

[†]Mission Design and Navigation Section, Jet Propulsion Laboratory, California Institute of Technology, 4800 Oak Grove Dr., Pasadena, CA 91109, (818) 354-0961, timothy.p.mcelrath@jpl.nasa.gov

[‡]Outer Planet Mission Analysis Group, Mission Design and Navigation Section, Jet Propulsion Laboratory, California Institute of Technology, 4800 Oak Grove Dr., Pasadena, CA 91109, (818) 354-1509, anastassios.e.petropoulos@jpl.nasa.gov

composition of Phobos are not known in detail and, therefore, a complete mapping of the surface is highly desirable. On the other hand, the relatively small size of Phobos compared to Mars itself poses an additional complication in the long-term stability of Phobos-centric orbits. Accordingly, we select distant retrograde orbits (DROs) as the nominal mapping trajectories of Phobos due to their well-known stability characteristics.[4] This security in the spacecraft path comes, however, at the cost of losing polar coverage during the orbiting phase of the mission. To overcome this deficiency we conduct a flyby campaign of the moon's poles prior to capture about Phobos, making use of the solar electric propulsion system to adjust the orbital parameters for successive flybys.

The dynamical environment near Phobos, heavily influenced by the perturbing presence of Mars, along with the irregular shape of the moon itself yields diverse opportunities for low-cost capture. However, the potential to exploit low-energy, multi-body effects also presents increased risk in the form of relatively rapid impacts or escapes in off-nominal scenarios. The perturbing influence of solar radiation pressure, while not explored in the present investigation, would add another complication to the generation of the trajectory. Furthermore, this region of complex dynamics in the vicinity of Phobos also necessitates the use of higher fidelity models and extensive numerical simulations, even for preliminary mission design and analysis. Thus, careful consideration of the nominal capture and walkdown sequence is desirable in order to balance ΔV and time savings with increased risk from close proximity to the surface of Phobos.

Because low-cost captures often entail close approaches to the irregularly-shaped Phobos, orbit determination and maneuver errors are of particular concern. This calls for in-depth analysis, even for preliminary trajectory designs. For certain nominal capture scenarios, even small perturbations in the applied thrust can result in impact with or escape from Phobos on the time scale of weeks. For the same reference paths, 3-σ errors leave only a few days for potential recovery before either escape or the crash of the robotic spacecraft. These dire warnings aside, there is indeed hope for a prospective mission, as the complex dynamical environment usually affords an opportunity for a rapid recovery either into a stable capture orbit or into a trajectory that safely escapes Phobos. In the event of a safe escape, the spacecraft has the potential for a return to Phobos and another attempted capture.

ANALYSIS SOFTWARE

A variety of analysis tools are used to construct the trajectories in this investigation, from the polar flybys to the capture and high and low mapping orbits (Hi-MO and Lo-MO, respectively). We will discuss these trajectories in more detail later, but what follows is a brief description of the relevant simulation software. The Small Body Dynamics Toolkit (SBDT) is a collection of MATLAB code that has been under development since 2001, first at the University of Michigan, then at JPL.[5] We also used the Mission-design and Operations Navigation Toolkit Environment (MONTE),[6] a multi-mission navigation and mission design software package developed and maintained at JPL. Finally, we developed a low-overhead Perl script, *phobints*, to perform simplified, analytical calculations when so desired.

DYNAMICAL MODELS FOR TRAJECTORY DESIGN

We employ a variety of different models for the gravitational dynamics in the Mars-Phobos region. While the implementations differ in their specific details, in general all simulations incorporate multi-body dynamics including both Mars and Phobos. Likewise, the highly non-spherical shape of Phobos is always captured, though to differing levels of fidelity depending on the specific

©2015 California Institute of Technology. Government sponsorship acknowledged.

cases under consideration. However, non-gravitational forces such as solar radiation pressure are not considered during this preliminary analysis.

For the flybys and mapping orbits, we use a polyhedral gravity-field model for the moons, based on shape models for Phobos.[7] We specify a constant density of 1.8458e12 kg/km^3, where this value is derived from the volume of the shape models and the GM values listed in Table 1, which are adapted from Jacobson.[8] The number of vertices in the Phobos model is 1538. In designing flybys and mapping orbits for the moon, Phobos is assumed to have a circular, equatorial orbit around Mars and only Phobos' gravity and Mars' gravity were included in the numerical integration. The rotational and orientation model used for the moon is libration-free, tidally locked, and body-fixed.

Table 1. Parameters for satellite flybys and Hi- and Lo-MOs.

Parameter	Value	Unit
Mars GM	42828.31	km^3/s^2
Phobos orbital radius	9378.314	km
Phobos GM	7.05482e-4	km^3/s^2

The capture analysis is performed using spherical harmonics gravitational models for Mars and Phobos and the point masses of the Sun and Deimos. The positions and masses of the gravitating bodies are extracted from the de405 and mar097 ephemerides. We used a 50x50 truncation of the MGS75E gravity field for Mars, while for Phobos we used 3x3 harmonics truncated from a shape-based gravity model.

For the Mars-centric thrust arcs targeting the polar flybys of Phobos, we employ a distributed-mass model for Phobos using the moon's average triaxial ellipsoid shape. For this analysis phase, the Phobos ephemeris is modeled as a conic. Even though the J_2 and higher spherical harmonics of Mars are not included, anything in a similar orbit to Phobos will receive very similar perturbations, and so they will make relatively small difference in the relative motion. While the triaxial ellipsoid only approximates the shape of Phobos, this assumption is much better than a point-mass model and delivers quite similar behavior to the polyhedral and spherical harmonic models.

DESTINATION ORBITS: HI-MO AND LO-MO

A prime goal of the Phobos orbiter is to map the Martian moon in sufficient detail to permit scientific characterization of Phobos surface features as well as enable selection of future landing sites. To this end, two mapping orbits, high and low, are constructed. The Phobos High Mapping Orbit (Hi-MO) is designed to afford coverage of as high latitudes as possible while still maintaining stability. In particular, the trajectory is robust to perturbations of 10 cm/s, spherical, to the initial velocity, meaning that it will neither impact nor escape from Phobos for at least 30 days. The mapping orbits, which have no deterministic ΔV, can be thought of as inclined DROs about Phobos, though in this case "distant" is a relative term. The Phobos Low Mapping Orbit (Lo-MO) is designed in the same manner as the Hi-MO and has the same stability characteristic of having a 10 cm/s spherical perturbation tolerance. The initial states, given in a Phobos-centered radial-tangent-normal (RTN) frame, for Hi-MO and Lo-MO are listed in Table 2, while the orbits are depicted in Fig. 1 where Hi-MO is red and Lo-MO is green. The RTN frame is defined with the "radial" directed from Mars to Phobos, the "normal" being perpendicular to Phobos' orbital plane, and "tangent" completing the right-handed set and being generally directed along Phobos' velocity direction.

©2015 California Institute of Technology. Government sponsorship acknowledged.

Table 2. Initial states and periods for Phobos Mapping Orbits. RTN frame, cartesian Phobos-centered coordinates. β is the Sun-Phobos-spacecraft angle.

Mapping Orbit	State (x, y, z) (km) (dx, dy, dz) (m/s)	Relative (hrs)	Inertial (hrs)	β-angle (hrs)
Hi-MO	-18, 0, 0 0.05, 11.9, 1.95	3.80	7.53	13.68
Lo-MO	-15, 0, 0 0, 11.48, 2.02	3.03	5.00	14.96

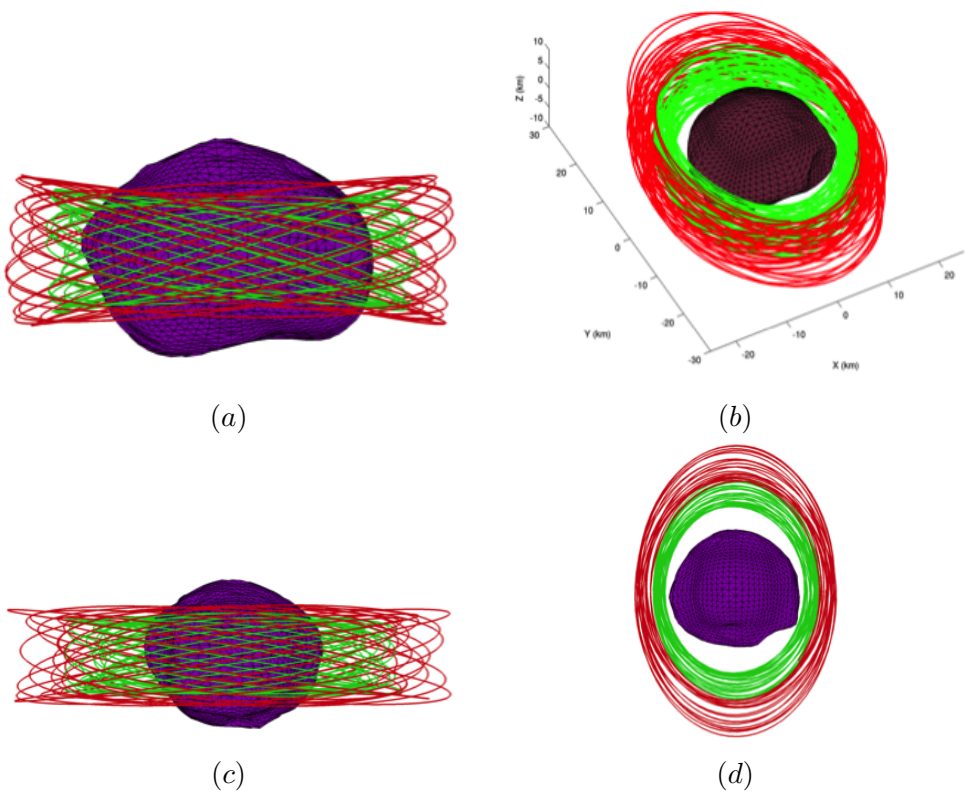

Figure 1. Phobos Hi-MO (red) and Lo-Mo (green) shown in the Phobos body-fixed frame. a. xz-projection; b. 3D view; c. yz-projection; d. xy-projection.

©2015 California Institute of Technology. Government sponsorship acknowledged.

The large J_2 value of Phobos, as well as the Mars perturbations, cause an interesting pattern for various periods of interest. Table 2 shows three periods for Phobos Hi-MO and Lo-MO. The retrograde motion drives the relative period (how often the same longitude is reached) to be less than the inertial period. The beta angle period describes how long the orbit plane takes to complete a revolution. It is quite fast! (An equivalent value for a 28.5-deg LEO orbit would be $\sim$50 days.) The orbit period of Phobos (459.2 minutes) drives the lighting conditions, and the combination drives the Sun-Phobos-spacecraft angle, β, to repeat every $\sim$79 hours, whereas the equivalent Hi-MO repeat pattern is a little over a week. This repetition is illustrated in Fig. 2, where the red line indicates the ground track of the spacecraft in Lo-MO over the 79 hour interval; a similar plot for the Hi-MO trajectory is not shown, as the ground tracks are qualitatively similar. Note that while coverage of the equatorial regions of Phobos is dense in Lo-MO, the polar regions are not accessed at all. The behavior in Hi-MO is little better, where the equator is covered in detail, but the spacecraft ground track does not extend to higher latitudes. This lack of polar coverage during the mapping phase necessitates the use of polar flybys of Phobos prior to capture into the Phobos-centric orbits.

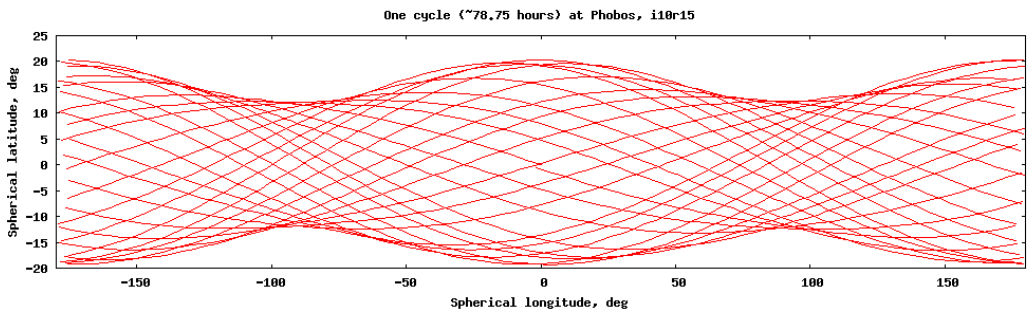

Figure 2. Phobos coverage of Lo-Mo over one period of illumination conditions, shown in spherical longitude and latitude. Even with the highly non-spherical shape of Phobos, significant portions of the poles remain uncovered.

POLAR COVERAGE VIA CLOSE FLYBYS

The spacecraft conducts two flavors of polar flybys at Phobos: 20-km altitude flybys for wider imaging coverage, and, once a sufficient portion of the 20-km flyby campaign has been conducted, 1-km altitude flybys for gravity science (plus whatever bonus imaging can be done). The 20-km flybys are along the Phobos RTN $\pm$X axis (collinear with the radial vector from Mars). They use a back-and-forth rotation pattern about the Y-axis (which is parallel to the direction of motion) to obtain a wider swath width. Assuming a 20% overlap in the ground coverage between flybys, a minimum of three passes per pole are required to fully image the polar regions. In order to make sure everything is illuminated, a set of three flybys is performed in each direction (+X and -X velocity) with the Sun on opposite sides (+Y and -Y). Some examples of 20-km flybys at the Phobos South pole are shown in Fig. 3.

The 1-km flybys may be in either the $\pm$X or $\pm$Y directions; in both cases, our intent is to bring the spacecraft as close to the surface as possible for as long a time as possible. At the 1-km level, the topography determines how close we can get, and often there are "hills" that determine the minimum altitude and "valleys" in between that consequently have higher altitudes. Sometimes an approach from a different direction allows the spacecraft to fly through the "valley" to get better measurements. A selection of 1-km polar flybys is depicted in Figs. 4 to 6. The flybys were designed

©2015 California Institute of Technology. Government sponsorship acknowledged.

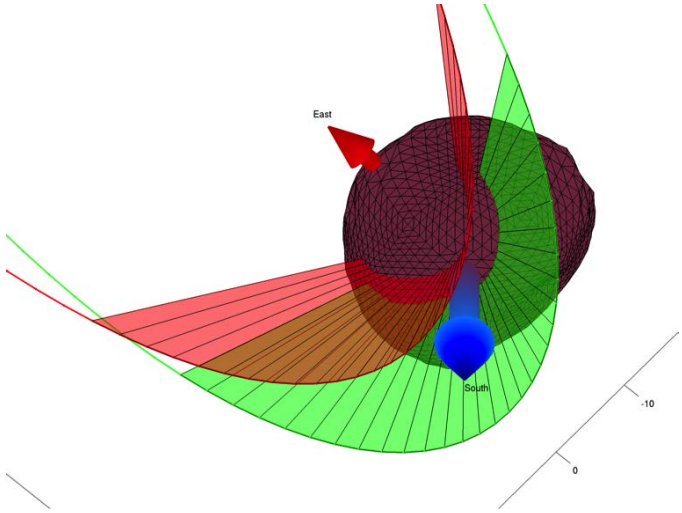

Figure 3. Phobos 20-km South pole flybys with 1.6-km Easterly and Westerly ground-track offsets; 4-minute tic marks.

by propagating the trajectory forwards and backwards in time from a point at or near what may be thought of as the "hyperbolic periapsis", i.e. what would be the periapsis point if Phobos were a point mass and the flyby trajectory were a hyperbola. This would typically be a point on or near the pole, with a velocity perpendicular or almost perpendicular to the radius vector from Phobos' center of mass. The initial states for both the 20-km and 1-km flybys are listed in Table 3.

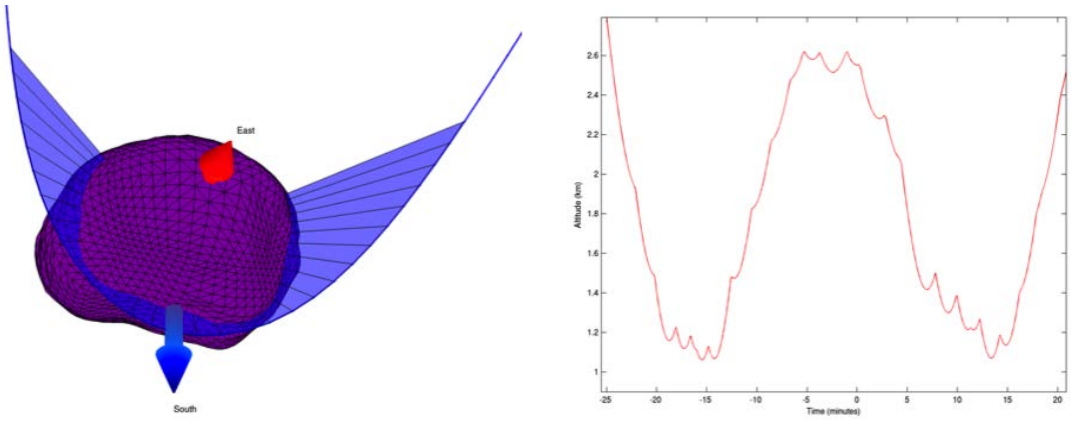

Figure 4. Phobos 1-km South pole flyby, along the prime-meridian plane. Trajectory with 4-minute tick marks on left, range to nearest vertex (aka "altitude") on right.

Lower flyby velocities were favored (in so far as the resulting trajectory maintained a sufficient altitude above the topography), both because it will simplify the operation of any associated scientific observations and because it results in smaller changes in the pre- and post-flyby areocentric orbits. The 20-km flybys maintain their altitude with 8 m/s, but the 1-km flybys require higher velocities. In particular, reaching low points in the topography may require nearly a 50% increase in velocity, as with the second flyby example in Table 3.

If the low flybys sound a little scary, do not be alarmed! First and foremost, the 20-km flybys will have already adequately mapped the surface features of the moon to enable proper planning of the

©2015 California Institute of Technology. Government sponsorship acknowledged.

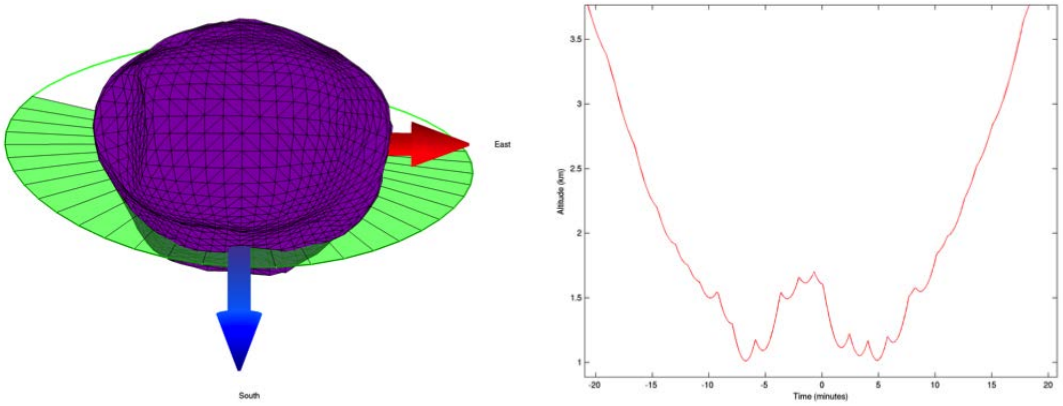

Figure 5. Phobos 1-km South pole flyby, east-west "through the valley". Trajectory with 4-minute tick marks on left, range to nearest vertex (aka "altitude") on right.

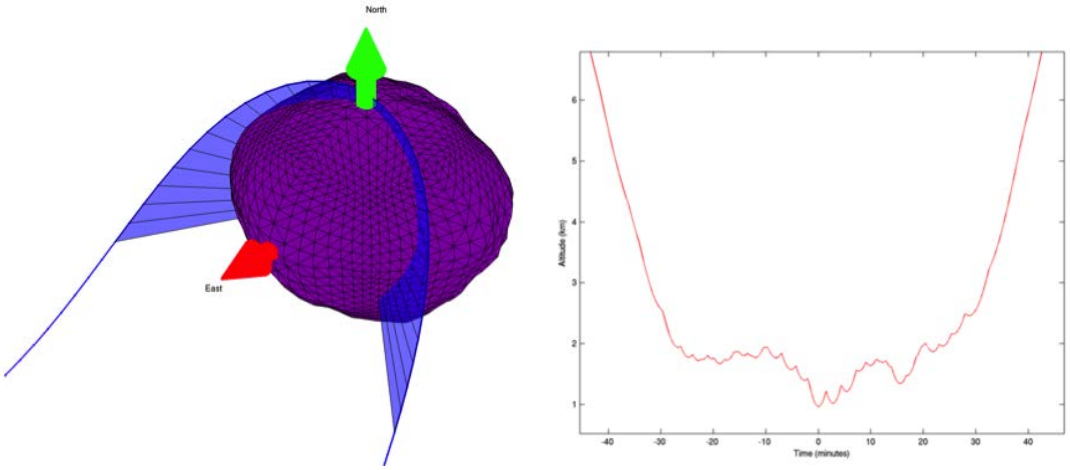

Figure 6. Phobos 1-km North pole flyby, along the prime-meridian plane. Trajectory with 4-minute tick marks on left, range to nearest vertex (aka "altitude") on right.

©2015 California Institute of Technology. Government sponsorship acknowledged.

Table 3. "Hyperbolic Periapsis" states for Phobos flybys. RTN frame, cartesian coordinates with respect to the center of Phobos.

Flyby	1-km S. Pole	1-km S. Pole, valley	20-km S. Pole, east offset	20-km S. Pole, west offset	1-km N. Pole
State (x, y, z) km	0, 0, -10.9	0, 0, -9.8	0, -5.904, -29.5	0, 5.904, -29.5	0, 0, 10.9
(dx, dy, dz) m/s	10, 0, -0.5	0, 12, 0.5	8, 0, 0	8, 0, 0	9, 0, 0

lower flybys. Secondly, the series of maneuvers that set up each flyby have their best performance in the radial and normal (i.e. altitude, for a polar flyby) directions, and are much worse in the downtrack directions. The assumed maneuver execution error model is 1 mm/sec and 1% proportional, both spherical and 3-sigma. For a final statistical targeting maneuver at E-12 hours of 36 cm/sec, the error is 3.74 mm/sec (here we define E-0 as the flyby epoch, i.e., the point of closest approach to the local terrain features). This maneuver error maps to $\sim$484 m of downtrack error, but only $\sim$16.4 m of normal error and $\sim$33 m of radial error, due to the orbital mechanics. In the case that the E-12 hour maneuver is missed, the previous maneuver could be as large as 6 m/s, centered at E-3 days. While the downtrack error from that maneuver would be 47 km, the normal and radial errors would be 263 m and 526 m respectively, and would not pose any impact threat for a 1-km polar flyby, for an approach with a plane difference of less than 0.5 degrees (which is always the case).

Each polar flyby changes the orbit of the spacecraft about Mars. For the 20-km flybys, the approach is from a small period offset (with respect to Phobos), and the flyby essentially reverses the offset (i.e. from longer period to shorter period), thus sending the spacecraft away. The flyby also changes the orbit plane and the eccentricity, both of which (along with the period) must be corrected back to the previous values, to set up another similar flyby.

This correction is accomplished in two deterministic maneuvers, one from E+2.5 to E+4 days after the previous flyby, and one from E-3.5 to E-2.5 days before the next flyby. In between are 2 days to update the next maneuver. After the second deterministic maneuver there are 2 days to develop the statistical maneuver at E-12 hours, followed by the flyby (E-0). This total cycle for the Phobos southern summer solstice polar flybys is 9.5 days long, due to the increased solar energy available for the SEP system. For the northern summer solstice (near aphelion), an extra day must added to each maneuver (to account for lower available power), for a total cycle of 11.5 days. With these durations, there is time allocated for 14 flybys at each Phobos pole/season, where this ability to conduct the flyby campaigns at any time throughout the Martian year increases operational flexibility.

While the period can be adjusted at any point in the orbit, the orbit plane can only be adjusted efficiently at two points, and the eccentricity vector adjustment has similar constraints (if radial control is being used, assuming the period is also being corrected throughout). Since low-thrust propulsion systems are not generally built for impulses, a control scheme must be assumed for correcting each parameter, and then applied to the differences between the pre- and post-flyby orbital elements to see if there is enough time to accomplish the change. For simplicity, we have used the following analytic approach to bound the problem, rather than solving a particular set of transfers with an optimizer. All aerocentric orbits are near-circular (eccentricity < 0.02) which greatly simplifies the problem.

The control scheme uses a fixed radial (k_r) or normal (k_n) component from the velocity (or anti-velocity) vector, maintained for 120 degrees around each of two opposite points in the orbit (where

©2015 California Institute of Technology. Government sponsorship acknowledged.

an impulse is most efficiently applied). The in-plane offset provides eccentricity vector control and the out-of-plane offset performs orbit plane control. If we pessimistically assume that both regions fall on top of each other and that the thrust offset instantaneously returns to zero outside the 120 deg arc, one can easily show that:

$$\|\Delta\hat{u}_h\| = \frac{\sqrt{3}}{\pi}\frac{\Delta v_p}{V}k_n \text{ radians} \tag{1}$$

$$\|\Delta\vec{e}\| = \frac{\sqrt{3}}{\pi}\frac{\Delta v_p}{V}k_r \tag{2}$$

where Δv_p is the ΔV per rev, V is the orbital velocity, $\hat{u}_h$ is the orbit pole direction, and $\vec{e}$ is the eccentricity vector. Over several revs, Δv_p is just the total low thrust ΔV. Note that part of the $\sqrt{3}/\pi$ factor is due to only thrusting in a useful direction for $2/3$ of a rev, and the rest is due to cosine losses. For semi-major axis control, one can show that if the offsets are (pessimistically) maintained throughout a full revolution, the semi-major axis change Δa is:

$$\Delta a = \frac{2a\Delta v_p}{V}\sqrt{1 - k_r^2 - k_n^2} \tag{3}$$

Obviously this implies a constraint on the values of k_r and k_n. Optimistically (with instantaneous slews to and from offsets that are over exactly the same arc), Δa could be at least as high as:

$$\Delta a = \frac{2a\Delta v_p}{V}\left(\frac{1 + 2\sqrt{1 - k_r^2 - k_n^2}}{3}\right). \tag{4}$$

For the impulsive case at the optimal point, these equations become:

$$\|\Delta\hat{u}_h\| = \frac{\Delta v_n}{V} \text{ radians} \tag{5}$$

and

$$\|\Delta\vec{e}\| = \frac{\Delta v_r}{V} \text{ radians} \tag{6}$$

where Δv_n is normal ΔV and Δv_r is radial ΔV. Of course, $\vec{e}$ is more easily changed by tangential ΔV, but we assume that all the tangential thrusting is being consumed by the period change. So the penalty for low thrust is an applied scale factor of 0.55 for normal and radial ΔV values, for this simple scheme.

For two sets of orbital elements, the differences need to be expressed in terms of $\Delta\hat{u}_h$ and $\Delta\vec{e}$. The pole unit vector, in terms of inclination i and the longitude of the ascending node Ω, is:

$$\hat{u}_h = \begin{bmatrix}\sin i \sin\Omega & -\sin i\cos\Omega & \cos i\end{bmatrix}^T \tag{7}$$

The angular difference between the pole vectors is:

$$\Delta h = \sqrt{1 - \hat{u}_{h_1}\cdot\hat{u}_{h_2}} \tag{8}$$

The eccentricity vector is approximately:

$$\vec{e} = e\cos(\omega + \Omega)\hat{x} + e\sin(\omega + \Omega)\hat{y} \tag{9}$$

and so

$$\Delta\vec{e} = \vec{e}_1 - \vec{e}_2 \tag{10}$$

©2015 California Institute of Technology. Government sponsorship acknowledged.

for nearly co-planar, nearly-circular orbits. With these parameters, we can now compute the low thrust maneuver durations required between any pair of polar flybys for this sub-optimal scheme.

There are 4 types of flybys considered here: 20-km +DX, 20 km -DX, 1-km +DX, and 1-km +DY. Naturally, the 20-km flybys have smaller changes from the encounter than the 1-km flybys. However, the subsequent 1-km flyby is not sensitive to lighting changes and so the node does not need to be corrected, greatly reducing the ΔV. A special case is switching from +X to -X flybys at 20-km, since the desired sun direction (and hence the location in the Phobos orbit) changes by 180 degrees. This both changes the plane significantly, and requires an approach from the other direction (in terms of period difference). Fortunately, a Y-axis flyby accomplishes that change fairly effectively. The 20-km flybys should be as close to the solstice as possible, so the probable pattern would be three -DX 20-km flybys, a Y-axis flyby at the solstice, and then three +DX 20-km flybys (or vice versa). The rest of the flybys (7 remaining) that are farther away from the solstice would need to include the other four 1-km flybys, leaving three close passages for margin or bonus observations.

A subset of the pattern around the solstice was run to make sure that the ΔV requirements (mainly in time) were met. The model inputs for the flyby targeting analysis are given in Table 4. Each flyby started at either Z=-29 km (for the 20-km flybys) or Z=-10.2 km (for the 1-km flybys). The 20-km velocity was always 8 m/s (in $\pm$DX) and the 1-km velocity was always 10.5 m/s (+DY or +DX). The flybys were integrated forward and backwards from the pole and then compared. Two -DX 20-km flybys before the solstice were followed by a +Y flyby at the solstice, and then a +DX 20-km flyby afterwards. Following that there are two 1-km +DX flybys. This covers every type of connection between different flavors of polar flybys at least once. (The actual sequence would have three same-direction 20-km flybys in a row on either side of the solstice). This sequence was run at the Phobos southern summer solstice of June 7, 2024, but could just as easily apply to the following solstice (except with more time between flybys due to only having reduced steady-state power for the SEP module). The time of the flyby at the solstice was adjusted to put the Sun close to the +Y Phobos RTN axis, but for simplicity the times of the 20-km flybys were not adjusted for the 0.5-deg/day motion of the Sun with respect to Mars, which would only have a small effect on the ΔV.

Table 4. Parameters for simulations of the polar flyby campaign.

Parameter	Value	Units
Phobos initial state (EME2000):		
Epoch	6/7/2024 00:00	
Semi-major axis	9378.9644	km
Eccentricity	0.015559	
Inclination	36.60253	deg.
Arg. of periapsis	-49.79144	deg.
Long. of asc. node	46.07288	deg.
Time from periapsis	-520.84	sec
Mars Gm	42828.28659	km^3/s^2
Phobos Gm	7.09174e-4	km^3/s^2

©2015 California Institute of Technology. Government sponsorship acknowledged.

The times of all the flybys and the orbital elements (other than the true anomaly) before and after the swingby are given in Table 5. The orbital elements are in the Phobos IAU system (fixed because Phobos is being propagated conically), where the z-axis is the Phobos orbit pole of date; the x-axis is the cross product of $\hat{z}$ with the Earth Mean Pole of J2000; and the y-axis completes the right-handed triad.[9] The maneuvers in between the flybys must change the orbital elements across the black lines of the table. As can be seen in Table 6, a combination of serendipity and nefarious intent keep the orbit plane and the eccentricity vector differences relatively small, reducing the total ΔV, while accepting a noticeable semi-major axis difference. The ΔVs on the table are for impulsive maneuvers in the optimal direction (i.e. tangential for semi-manor axis and eccentricity), and so must be divided by 0.55 for plane change and 0.276 for radial eccentricity control using low thrust (in 120-deg arcs, as discussed above).

To illustrate the orbit correction sequence between each successive flyby, we examine the first transfer in detail. The first maneuver should perform 2.65 m/s of downtrack ΔV (about half the semi-major axis difference) and (if possible) all of the orbit plane adjustment (to reduce the magnitude and errors of the second maneuver), which is 8.63 m/s (after dividing by .55) of normal ΔV (in terms of full revs of thrusting). The eccentricity vector change is inconsequential, and can be handled efficiently by adjusting the start and stop times of the downtrack thrusting of the second maneuver. The 1.5-day duration allocated for the first maneuver covers approximately 4.7 orbit periods, so we could perform 2.41*4.7 = 11.33 m/s of equivalent plane change ΔV if the phasing was ideal. Instead, we divide the required thrusting over 4 periods, which is 2.16 m/s per rev, and the normal component is 0.896. That leaves a factor of .444 for tangential thrusting, and if that was only applied during the two 120-deg arcs, that would still be 2.85 m/s of tangential ΔV, which is slightly more than is necessary, without even using the other two 60-degree arcs. (A more optimal transfer would slightly reduce the 120-deg arcs, such that the required normal and tangential components matched exactly). Clearly this case has plenty of margin. The total applied ΔV is around 9 m/s.

Table 5. Orbit element differences caused by a subset of polar flybys, in Phobos IAU frame.

State type	Flyby & Epoch	Semi-major axis, km	Eccentricity	Inclination, deg.	Arg. of perifocus, deg.	Long. of node, deg.
Pre-flyby state	1st 20-km -DX	9402.21	0.0133	0.2069	159.758	150.310
	-60 revs					
Post-flyby state	5/18/24 22:28:00 ET	9355.68	0.0134	0.2091	-165.299	114.697
Pre-flyby state	2nd 20-km -DX	9402.21	0.0133	0.2069	159.753	150.315
	-30 revs					
Post-flyby state	5/28/24 12:16:30 ET	9355.68	0.0134	0.2091	-165.304	114.701
Pre-flyby state	1-km +DY	9414.58	0.0171	0.1382	-159.052	111.737
	-1/4 revs					
Post-flyby state	6/07/24 00:10:00 ET	9414.57	0.0171	0.1382	-22.870	-29.210
Pre-flyby state	20-km +DX	9355.68	0.0134	0.2092	-17.253	-32.090
	+29.5 revs					
Post-flyby state	6/16/24 12:03:42 ET	9402.21	0.0133	0.2070	17.643	-67.659
Pre-flyby state	1st 1-km +DX	9343.72	0.0163	0.1669	23.568	-72.724
	+60.25 revs					
Post-flyby state	6/26/24 07:36:54 ET	9414.46	0.0148	0.1669	155.568	155.207
Pre-flyby state	2nd 1-km +DX	9343.47	0.0153	0.1641	146.277	161.365
	+89.9 revs					
Post-flyby state	7/05/24 18:44:32 ET	9414.97	0.0161	0.1653	-79.567	31.694

©2015 California Institute of Technology. Government sponsorship acknowledged.

Table 6. ΔV for transfers between sample flybys.

Parameter	#	Transfer	Semi-major axis	Orbit Plane	Ecc. vector
Difference	1	1st 20-km -DX flyby to	46.53 km	0.1273 deg	0.00017
Ideal ΔV cost		2nd 20-km -DX flyby	5.305 m/s	4.748 m/s	0.185 m/s
Difference	2	2nd 20-km -DX flyby to	58.90 km	0.0714 deg	0.00376
Ideal ΔV cost		1-km +DY flyby	6.715 m/s	2.666 m/s	4.021 m/s
Difference	3	1-km +DY flyby to	58.89 km	0.0715 deg	0.00376
Ideal ΔV cost		20-km +DX flyby	6.714 m/s	2.668 m/s	4.018 m/s
Difference	4	20-km +DX flyby to	58.49 km	0.0433 deg	0.00296
Ideal ΔV cost		1st 1-km +DX flyby	6.668 m/s	1.617 m/s	3.170 m/s
Difference	5	1st 1-km +DX flyby to	70.99 km	0.0180 deg	0.00098
Ideal ΔV cost		2nd 1-km +DX flyby	8.094 m/s	0.671 m/s	1.049 m/s

CAPTURE INTO PHOBOS-CENTRIC ORBIT

We now turn to the baseline concept of operations for initial capture around the Martian moon Phobos. Capture operations include the initial insertion into loose capture around Phobos as well as the transfer process down to the first science orbit (Hi-Mo). Furthermore, we discuss contingency options for 3-σ thrust errors as well as missed thrust events.

Throughout the capture analysis, states and maneuvers are typically expressed in the Phobos RTN of instant frame, which is inertial because the axes are considered to be instantaneously inertial for the purposes of transforming velocity terms. Thus, centripetal and Coriolis terms are not relevant during transformations between the Phobos RTN of instant frame and other inertial frames. The altitudes were computed as bodydetic altitudes, i.e., distance to the nearest surface point, with respect to a triaxial ellipsoid, given in Seidelmann et al.[10] All of the dates are for a time before actual Phobos arrival, but the qualitative behavior of the capture orbits should be largely invariant, and depend more on the true anomaly of Phobos than anything else.

Nominal Phobos Capture

The baseline approach to Phobos from a Mars-centered orbit is composed of an inbound coast to the vicinity of Phobos followed by a quasi-capture about Phobos. The inbound trajectory targets the rotating frame state shown in Table 7 where a trajectory hitting this nominal state remains in the vicinity of Phobos nearly 16 days before an eventual escape from Phobos. Four days after achieving the target state, a stabilizing capture burn, also displayed in Table 7, is delivered by the ion engine with the thrust pointing direction expressed in the RTN of instant frame. The burn epoch is selected such that the maneuver occurs during a y=0 crossing of the trajectory, though this constraint is merely for design and illustrative purposes and does not imply an actual limitation on the spacecraft performance. This burn ensures that the spacecraft remains captured about Phobos for several months with no need for any additional maneuvers to prevent escape or impact. Note that all nominal capture and walk-down maneuvers, even though they are performed by the low-

©2015 California Institute of Technology. Government sponsorship acknowledged.

thrust engine, are small enough in magnitude that they are adequately modeled as finite burns that last on the order of tens of minutes.* The error recovery maneuvers, to be discussed later, also exhibit roughly the same behavior. The Phobos approach and stabilizing capture are illustrated in Fig. 7. In the figure, the red marker indicates the target state, whereas the green marker locates the deterministic capture burn. As displayed in Fig. 7(a), the stabilized capture trajectory after the maneuver presents more cohesive orbital behavior than the pre-burn quasi-capture. Furthermore, the stabilized capture yields lower apoapsis altitudes with respect to Phobos, as indicated in Fig. 7(b). Thus, with a relatively short impulse from the ion thrusters, the naturally occurring loose capture is readily converted to a longer-term capture presenting ample opportunity for altitude lowering to the target science orbits.

Table 7. Phobos capture orbit initial state and stabilizing burn. RTN of instant frame, cartesian Phobos-centered coordinates.

	Loose Capture State (x, y, z) (km) (dx, dy, dz) (m/s)	**Stabilizing Burn Magnitude (cm/s)**
Value	-15, 29.0389, -4.7290 -15.3126, 2.885, -1.39	5
Epoch	11-JUL-2022 12:37:08 ET	15-JUL-2022 16:38:18 ET

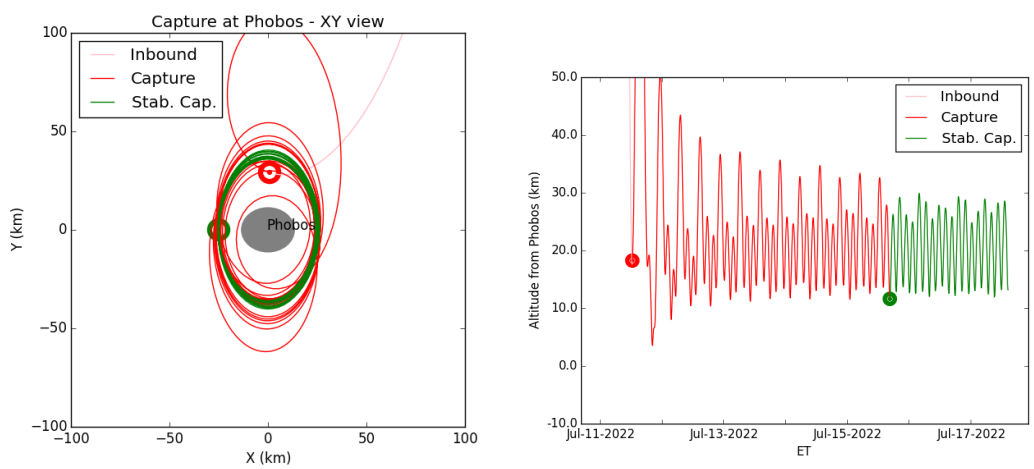

(a) **(b)**

Figure 7. Nominal approach and capture into Phobos-centric orbit, XY-projection and dedic altitude above Phobos surface (approximated as tri-axial ellipsoid). Red marker indicates target capture state whereas green marker indicates deterministic capture burn.

After the spacecraft is inserted into a stable orbit about Phobos, a sequence of burns progressively lowers the trajectory until the target science altitudes are reached. Furthermore, during this walk-down process, the DZ velocity component at the y=0 crossings may need to be adjusted in order to match the Hi-MO value. While a full set of walk-down burns is not detailed, a few steps illustrative of the full process are presented here. All burns occur at a y=0 crossing, unless otherwise indicated.

*All the nominal and recovery maneuvers were generated using the Terrestrially Regulated Iterative Algorithm for Learning and Estimation of Realistically Recognizable Operative Representations (TRIAL&ERROR).

©2015 California Institute of Technology. Government sponsorship acknowledged.

First, an "eccentricity increasing" burn that lowers the periapsis is performed, followed by a second maneuver to reduce the apoapsis. Alternately, rather than lowering the apoapsis, this second burn could be used to reduce the DZ component of velocity. Preliminary results indicate that the altitude lowering and DZ reduction maneuvers should occur separately in order for the maximal effects for each burn strategy to be realized. The three sample maneuvers are detailed in Table 8; note that these burns occur on two-day intervals, allowing sufficient time for the maneuvers to be fully designed.

Table 8. Walk-down maneuvers, in Phobos RTN of instant frame.

Parameter	"Eccentricity" burn	Burn #2, lower altitude	Burn #2, lower DZ
Epoch	17-Jul-2022 14:33:21 ET	19-Jul-2022 14:33:21 ET	19-Jul-2022 14:33:21 ET
Magnitude, cm/s	13.0	15.8	20.0

The trajectory and altitude for the two nominal capture and walk-down options, i.e., altitude lowering and DZ reducing, are shown in Fig. 8, along with the evolution of the X and DZ components of the Y=0 crossings that lie between Phobos and Mars. This sequence of images highlights both the similarities and differences between the two orbit lowering options. As can be seen in Fig. 8, the option to lower DZ brings the velocity component below the threshold value of 1.8 m/s, indicating that excessive Z excursions can be eliminated using only one thrust interval. For both cases, the apoapsis altitude is still above the 18 km altitude required for the science orbits, but a relatively quick pace of maneuvers (i.e., two-day intervals between deterministic burns) indicates that the target altitude is readily achieved in less than a month of operations. Furthermore, the strategy of alternating "eccentricity" and "lowering / stabilizing" maneuvers enables this rapid reduction in altitude with a relatively intuitive, operationally simple, and safe process.

Effect of Errors in Insertion Maneuver

The nominal capture and walk-down present a relatively efficient method to transfer from a Mars-centered orbit to the Phobos-centered science orbit. However, the multi-body effects of the Mars-Phobos system and the irregular shape of Phobos itself create a complex dynamical system influencing the motion of the spacecraft. Accordingly, contingency operations in the event of maneuver errors and missed thrust opportunities must be developed. While we do not develop a full complement of restoration options for this initial investigation, preliminary analysis indicates that 3-σ burn errors and missed thrust opportunities, even when they occur together, can be recovered from while ensuring the safety of the spacecraft. While the following error recovery case is examined using impulsive burn models, comparison between finite and impulsive burn results for the nominal capture indicate that a higher-fidelity finite burn model will not substantially alter the analysis of recovery options.

Before examining a specific contingency scenario, we consider the broad effect that thruster errors can have upon the initial approach to the loose capture around Phobos. A maneuver targeting the nominal insertion state is assumed to occur 1 day before the insertion epoch on 11 Jul-2022. The magnitude of this targeted burn is specified to be no larger than 10 cm/s such that the root sum of squares (RSS) of a proportional error term of 1% and a fixed error term of 1 mm/s comes to a 3-σ error of roughly 1.4 mm/s. In lieu of a full Monte Carlo analysis, we examine the effect of the error burn by performing a grid search over the $\pm$3-σ burn magnitude range for two fixed directions, namely DX and DY. Errors in the DZ direction are omitted since they do not significantly alter the baseline motion of the spacecraft. This grid search is sufficient for preliminary analysis because

©2015 California Institute of Technology. Government sponsorship acknowledged.

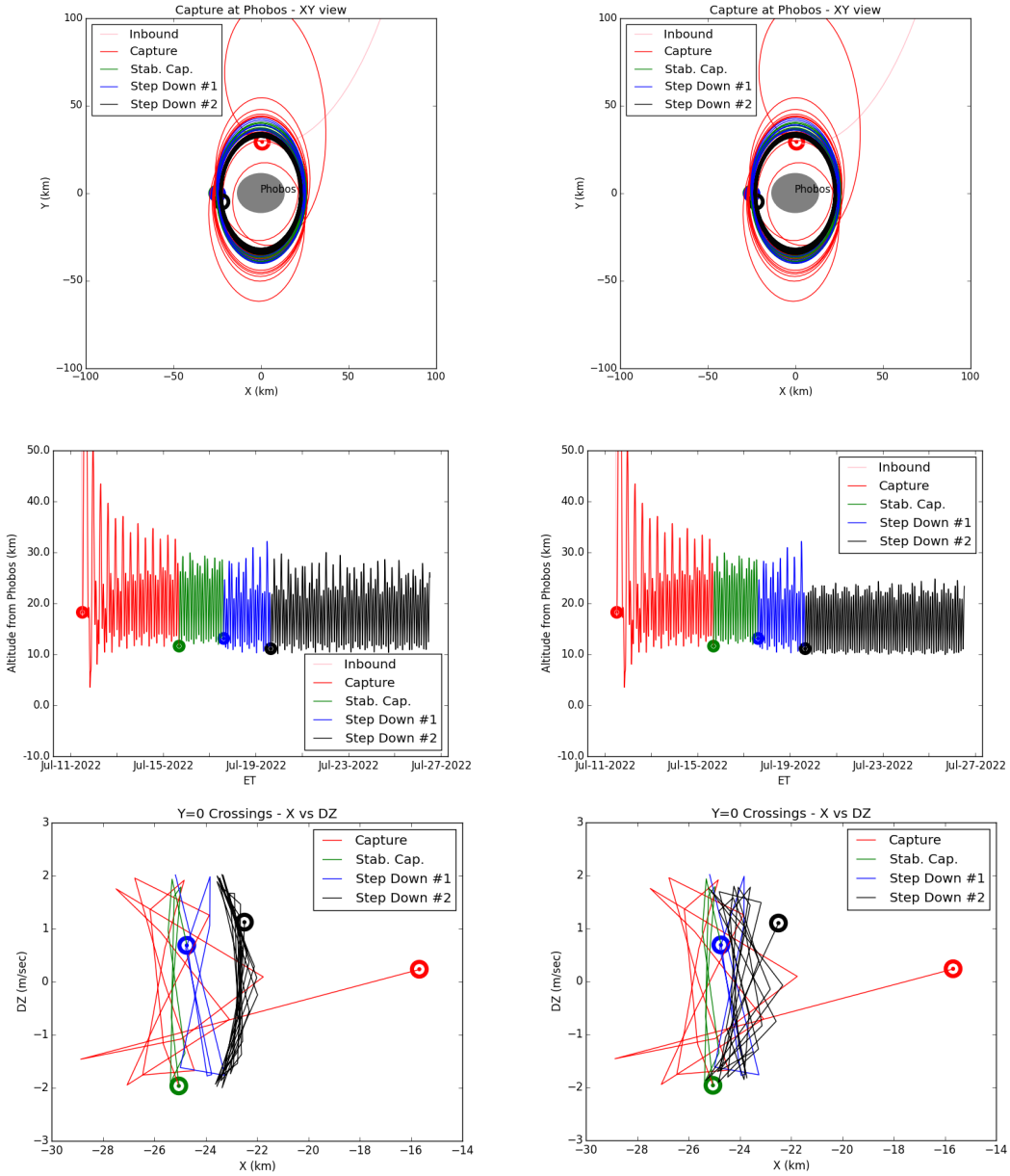

(a) **(b)**

Figure 8. Nominal walkdowns toward HiMo orbit for (a) altitude reducing strategy and (b) DZ reducing scheme. XY-projection, dedic altitude above Phobos surface (approximated as tri-axial ellipsoid), and X vs. DZ projections of the $Y = 0$ crossing occuring between Mars and Phobos. Red marker indicates target capture state whereas other colored markers indicate deterministic burns.

©2015 California Institute of Technology. Government sponsorship acknowledged.

it illustrates the statistical effect of insertion errors without undue computational burden. For each combination of burn magnitude and direction, we apply the error in the "targeting maneuver" to the baseline trajectory and propagate the motion of the spacecraft forward in time for 16 days. During this stage of the error analysis, we purposefully ignore the nominal capture and walk-down maneuvers so that we capture only the natural evolution of the spacecraft trajectory. Over these 16 days, we record any impact with the surface of Phobos (we model Phobos' shape as a triaxial ellipsoid in this scenario), with the results provided in Fig. 9. Note that the figure only displays the epochs of any *impact* with Phobos; if, instead, a particular combination of error magnitude and direction causes the spacecraft to escape the vicinity of Phobos within the 16 day interval, we do not record that information. As we can see, there is a distinct peak near the nominal burn with rapidly decreasing impact epochs as the error in the burn grows. Indeed, we see that the nominal approach is in fact rather sensitive to perturbations, with many impacts occuring within a few days of the nominal insertion epoch. On the other hand, as previously noted, this nominal approach requires relatively little impulse from the thruster in order to stabilize the capture, and usually, as we will show, relatively small maneuvers to correct the perturbed trajectory. Nonetheless, a more prudent balance of nominal performance and recovery options may be desirable.

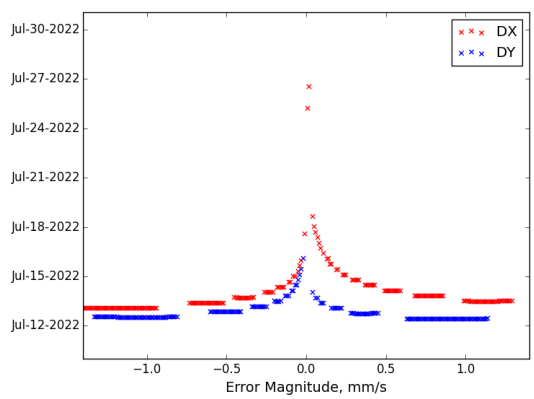

Figure 9. Epochs of Phobos impact due to burn errors in statistical maneuver on 10-July-2022 targeting Phobos insertion, one day prior to nominal insertion epoch of 11-July-2022.

Recovery Options

We turn now to an examination of potential recovery options in the event of an off-nominal approach to the Phobos capture. A statistical error of 1.29 mm/s in the +DX direction, representing the RSS of the constant error term and a proportional error term, is placed upon the notional 10-Jul-2022 burn, resulting in a perturbed trajectory. Note that this error magnitude, slightly below the 1.4 mm/s 3-σ bound for a 10 cm/s maneuver, was purposefully selected to ensure that the spacecraft would impact Phobos within two days of the nominal 11-Jul-2022 insertion epoch unless corrective action was taken. The resulting trajectory and altitude time history due to this "insertion error" maneuver is illustrated in Fig. 10. In the figure, red indicates the nominal insertion trajectory whereas green indicates the error case. Green markers indicate locations of the baseline (at nominal insertion epoch) and backup (1 day after nominal insertion epoch) recovery burns.

Assuming that an insertion error of some sort will occur, a nominal recovery burn is scheduled

©2015 California Institute of Technology. Government sponsorship acknowledged.

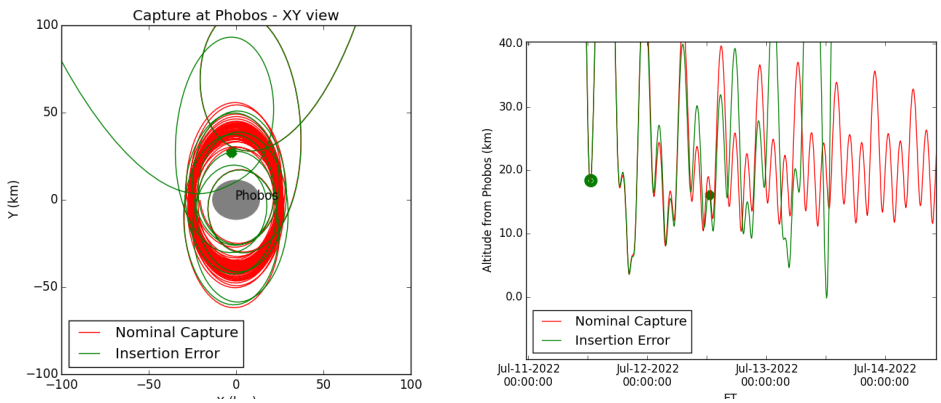

Figure 10. Phobos approach with error 1 day prior to nominal insertions, XY-projection and dedic altitude above Phobos surface (approximated as tri-axial ellipsoid). Note that, without recovery, impact occurs at approximately 12:00 13-July-2022.

for one day later on the original insertion epoch on 11-Jul-2022, with the elements provided in Table 9. We also determine a back-up case, to be discussed shortly, in the event the nominal burn is missed. The maneuver for this case (of magnitude 1.1 cm/s) rejects the applied disturbance and restores the spacecraft to a long-term quasi-capture from which the nominal stabilization and walk-down can commence as scheduled. Furthermore, even when subjected to 3-σ perturbations on the recovery maneuver, the resulting spacecraft trajectory provides at minimum two days of operational time for further recovery efforts. The recovery burn effect on the trajectory and altitude is shown in Fig. 11. In the event of 3-σ maneuver execution errors at the 11-Jul-2022 maneuver, the next statistical maneuver (a day later) would have a magnitude of 7 cm/sec in order to ensure stability.

Table 9. Recovery maneuvers, in Phobos RTN of instant frame.

Parameter	Baseline recovery	Backup recovery
Epoch	11-JUL-2022 12:37:08 ET	12-JUL-2022 12:37:08 ET
Burn Magnitude (cm/s)	1.08	13.4

While the recovery maneuver rejects the previous insertion error and allows for a restoration of the baseline capture behavior, the previously mentioned back-up maneuver is planned in the case of completely missing the nominal recovery maneuver. Thus, even if the nominal recovery cannot be achieved, the spacecraft can be prevented from impacting Phobos. However, this back-up burn of 13 cm/s, scheduled exactly one day after the 11-Jul-2022 insertion epoch (see Table 9), does not allow for the quasi-capture behavior to be accomplished. Instead, in order to avoid potential impacts with Phobos, the spacecraft is set on an escape trajectory from Phobos. While not desirable in terms of schedule, this escape at least prevents the loss of the spacecraft and permits another capture attempt at Phobos at a later date. The backup recovery burn's effect on the trajectory and altitude is shown in Fig. 12.

CONCLUSIONS

We have presented concepts and preliminary trajectory analysis for a solar electric propulsion enabled orbiter mission to explore the Martian moon Phobos. Specifically, we have detailed how

©2015 California Institute of Technology. Government sponsorship acknowledged.

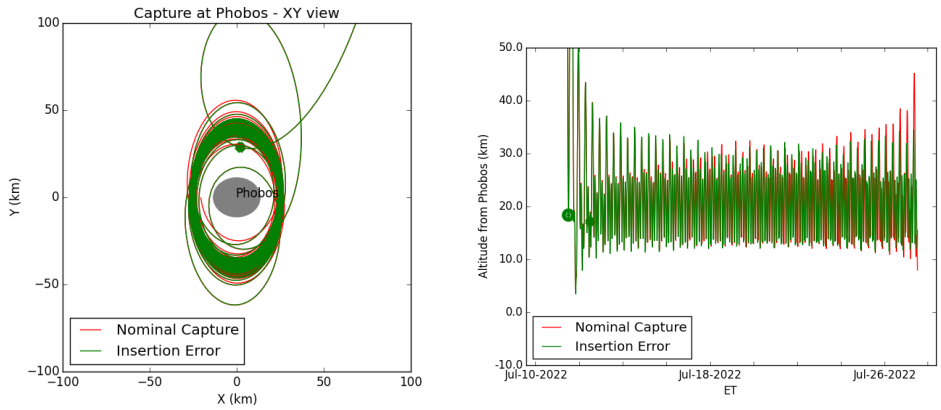

Figure 11. Phobos approach with error recovery at nominal insertion epoch, XY-projection and dedic altitude above Phobos surface. Color scheme is consistent with Fig. 10. Note that recovery burn stabilizes capture into a Phobos-centric orbit.

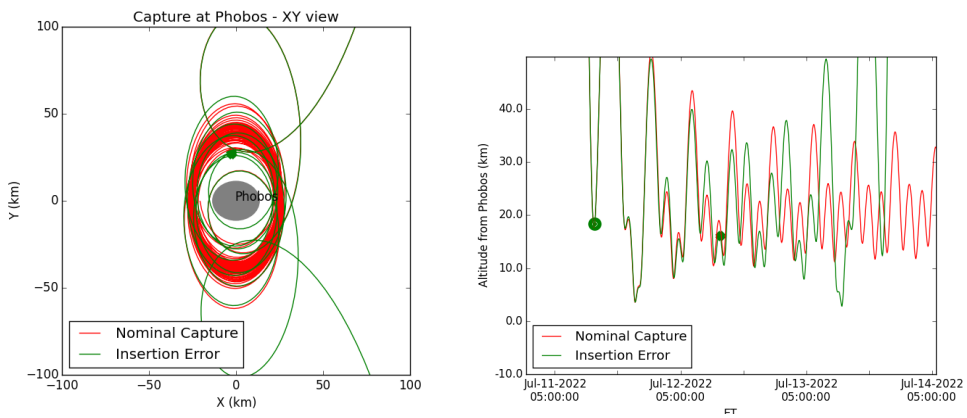

Figure 12. Phobos approach with error recovery at backup location, 1 day after nominal insertion epoch, XY-projection and dedic altitude above Phobos surface. Color scheme is consistent with Fig. 10. Note that spacecraft departs Phobos after backup burn but does not impact.

the entire surface of the moon can be characterized by a series of polar flybys followed by a capture into a set of mapping orbits about Phobos. Various dynamical models were used in different stages of the investigation, however all implementations sufficiently capture the non-spherical shape of Phobos as well as the multibody effects of Mars and Phobos for initial design phases. Both the high- and low-mapping orbits (Hi-MO and Lo-MO, respectively) provide ample coverage of the low latitudes of Phobos which, due to the irregular shape of the body, compose a large fraction of the surface area. In contrast, the polar regions of Phobos are accessed via a series of flybys, prior to capture into the final mapping orbits. Initial mapping of the polar regions is performed using 20-km altitude flybys, while closer surveys and gravity science can be conducted using lower 1-km flybys. In fact, some of these low flybys are specifically targeted to fly "through" the prominent valley on the moon's south pole (the authors cannot resist pointing out the analogy to the famous "trench run" scene from the original *Star Wars* film, though hopefully the only ion engines we will need to worry about are on our own spacecraft!). Between successive flybys, appropriate adjustments to the Mars-centered spacecraft orbit require only 10's of m/s in ΔV to implement. Once the flyby

©2015 California Institute of Technology. Government sponsorship acknowledged.

campaign has completed, the spacecraft captures into a Phobos-centric orbit and begins the walkdown sequence into the mapping orbits. The initial capture exploits Phobos and Mars multibody effects to naturally approach and insert into Phobos orbit, such that deterministic maneuvers are not required in the initial phases. However, the naturally occurring capture also necessarily entails an eventual departure, unless a small maneuver, on the order of cm/s, stabilizes the orbit. After the initial insertion, a series of "eccentricity increasing" and "restabilization" burns effect a walkdown to the target mapping orbits, where these maneuvers are typically small in magnitude (10's of cm/s) and afford several days between each thruster usage. Accordingly, we examine contingency options in the event of statistical maneuver errors and missed thrust opportunities. In all cases examined, recovery maneuvers can be constructed that, at minimum, remove the possibility of future impacts, even if the spacecraft must eject from Phobos orbit and make another capture attempt at a later date.

ACKNOWLEDGEMENTS

The work presented in this paper has been carried out at the Jet Propulsion Laboratory, California Institute of Technology, under a contract with the National Aeronautics and Space Administration.

REFERENCES

[1] S. Murchie, D. Britt, and C. Pieters, "The value of Phobos sample return," *Planetary and Space Science*, Vol. 102, 2014, pp. 176–182.

[2] P. Rosenblatt, "The origin of the Martian moons revisited," *Astronomy and Astrophysics Review*, Vol. 19, 2011, pp. 1–26.

[3] T. Duxbury, A. Zakharov, H. Hoffman, and E. Guinness, "Spacecraft exploration of Phobos and Diemos," *Planetary and Space Science*, Vol. 102, 2014, pp. 9–17.

[4] M. Henon, "Numerical exploration of the restricted problem. V. Hill's case: periodic orbits and their stability," *Astronomy and Astrophysics*, Vol. 1, 1969, pp. 223–238.

[5] S. B. Broschart, M. Abrahamson, S. Bhaskaran, E. G. Fahnestock, R. Karimi, G. Lantoine, T. A. Pavlak, and L. Chappaz, "The Small-Body Dynamics Toolkit and Associated Close-Proximity Navigation Analysis Tools at JPL," *AAS Guidance and Control Conference*, Breckenridge, Colorado, Jan. 30 - Feb. 4 2015. AAS Paper 15-127.

[6] R. F. Sunseri, H. C. Wu, S. E. Evans, J. R. Evans, T. R. Drain, and M. M. Guevara, "Mission Analysis, Operations, and Navigation Toolkit Environment (Monte) Version 040," tech. rep., NASA Tech Briefs, September 2012.

[7] R. Gaskell, "Gaskell Phobos Shape Model V1.0," 2011. Data Set ID: VO1-SA-VISA/VISB-5-PHOBOSSHAPE-V1.0, NASA Planetary Data System.

[8] R. Jacobson, "The Orbits and Masses of the Martian Satellites and the Libration of Phobos," *The Astronomical Journal*, Vol. 139, 2010, pp. 668–679.

[9] B. A. Archinal, M. F. A'Hearn, E. Bowell, A. Conrad, G. J. Consolmagno, R. Courtin, T. Fukushima, D. Hestroffer, J. L. Hilton, G. A. Krasinsky, G. Neumann, J. Oberst, P. K. Seidelmann, P. Stooke, D. J. Tholen, P. C. Thomas, and I. P. Williams, "Report of the IAU Working Group on Cartographic Coordinates and Rotational Elements: 2009," *Celestial Mechanics and Dynamical Astronomy*, Vol. 109, No. 2, 2011, pp. 101–135.

[10] P. K. Seidelmann, V. Abalakin, M. Bursa, M. Davies, C. de Bergh, J. Lieske, J. Oberst, J. Simon, E. Standish, P. Stooke, and P. C. Thomas, "Report of the IAU/IAG Working Group on Cartographic Coordinates and Rotational Elements of the Planets and Satellites: 2009," *Celestial Mechanics and Dynamical Astronomy*, Vol. 82, No. 1, 2002, pp. 83–111.

©2015 California Institute of Technology. Government sponsorship acknowledged.